GMAW焊接熔池形状和表面变形的数值模拟

孙永兴[1]，　翟　磊[2]，　赵　明[1]
（1. 中国石油大学 机电工程学院，山东 东营　257061；
2. 胜利油田胜利勘察设计研究院有限公司，山东 东营　257026）


孙永兴

摘　要：采用双椭球体热源分布模式，把过热熔滴带入熔池的热焓量处理为特定区域的均匀热源，建立了运动电弧下 GMAW焊接热过程的数值分析模型．利用 Visual Fortran编写数值计算程序，预测了从电弧引燃到准稳态过程中焊接熔池形状和熔池自由表面变形的动态演变，并进行了对比试验．基于数值模拟和工艺试验结果，可以看出达到宏观准稳态时计算所得的焊缝形状尺寸与试验结果基本吻合，因此验证了所建模型和采用的计算方法是正确、可靠的．

关键词：熔化极气体保护焊；表面变形；双椭球体热源；数值分析
中图分类号：TG444　　文献标识码：A　　文章编号：0253－360X（2010）10－0039－04

0　序　　言

熔化极气体保护焊（GMAW）是生产中广泛采用的焊接方法，具有焊缝质量好、可操作性强、生产效率高等优点，可用于各类金属材料的焊接[1]．对 GMAW焊接热过程进行数值分析时，焊接热输入主要包括两部分，一是焊接电弧作用于工件的热量，二是过热熔滴带入熔池的热量．合理建立焊接电弧在工件的分布以及熔滴热焓量在熔池内部的分布成为对 GMAW焊接热过程数值模拟的关键问题之一．

采用双椭球体热源分布模式，并把过热熔滴带入熔池的热焓处理为特定区域的均匀热源，利用 Visual Fortran编写数值计算程序，预测 GMAW焊接时熔池形状和自由表面变形的动态演变，并与试验结果进行对比．

1　数学模型

1.1　控制方程及定解条件

设焊接材料为各向同性，温度 $T(x, y, z, t)$为空间坐标（x, y, z）和时间 t的函数，x轴以焊接速度方向为正方向，z轴以熔池深度方向为正方向．

（1）在直角坐标系中，能量守恒方程为

$$\rho c_p\frac{\partial T}{\partial t}=\frac{\partial}{\partial x}\left(k\frac{\partial T}{\partial x}\right)+\frac{\partial}{\partial y}\left(k\frac{\partial T}{\partial y}\right)+\frac{\partial}{\partial z}\left(k\frac{\partial T}{\partial z}\right)+S_1+S_2 \tag{1}$$

式中：k为热导率；c_p为定压比热容；ρ为材料密度；T为温度；t为时间；S_1为内部热源；S_2为过热熔滴热焓．

（2）能量守恒方程的边界条件如下所示．

① 工件上表面：

$$k\frac{\partial T}{\partial z}=q_a-q_{cr}-q_{evp} \tag{2}$$

$$q_{cr}=\alpha_{cr}(T-T_a) \tag{3}$$

$$q_{evp}=m_{er}L_b \tag{4}$$

式中：q_a为工件上的电弧热流密度；q_{cr}，q_{evp}分别为对流和辐射、蒸发热损失；T_a为环境温度；m_{er}为蒸发率；L_b为液气相变潜热；α_{cr}为对流和辐射边界的综合散热系数．

② 工件下表面：

$$-k\frac{\partial T}{\partial z}=-q_{cr} \tag{5}$$

③ 计算区域关于焊缝中心线对称，有

$$\frac{\partial T}{\partial y}=0 \tag{6}$$

（3）能量守恒方程的初始条件为

$$T(x, y, z, 0)=T_a \tag{7}$$

1.2　熔池自由表面的变形

在焊接过程中，在电弧压力、熔滴冲击力、熔池重力及表面张力等的作用下，熔池的表面将产生变形．

收稿日期：2009－05－25
基金项目：中国石油大学博士科研基金资助项目（Y070305）．

设熔池上表面形状函数为 $\varphi(x,y)$，对于焊接过程中任一时刻，根据能量守恒原理，得未全熔透熔池自由上表面的变形方程为[2]

$$p_a-\rho g\varphi+p_d-\lambda=-\gamma\frac{(1+\varphi_x^2)\varphi_{yy}-2\varphi_x\varphi_y\varphi_{xy}+(1+\varphi_y^2)\varphi_{xx}}{(1+\varphi_x^2+\varphi_y^2)^{3/2}} \quad (8)$$

式中：p_a 为电弧压力；g 为重力加速度；p_d 为熔滴冲击力；λ 为拉格朗日常数；γ 为表面张力.

参考压力可以按下述方法确定，即变形前后熔池体积变化应该等于填充到熔池内的熔滴的体积之和.

$$\iint_{\Omega}\varphi\,\mathrm{d}x\mathrm{d}y=\Delta V \quad (9)$$

式中：Ω 为熔池上表面液相线所围成区域；ΔV 为单位时间内熔池体积变化量.

2 源项分布

2.1 双椭球电弧热流分布

电弧热源模型是实现焊接热过程数值模拟的基本条件之一. 文中采用双椭球状热源分布模式[3]，数学表达式为

$$q_f(x,y,z)=\frac{6\sqrt{3}(f_fQ)}{\pi\sqrt{\pi}a_1bc}\exp\left[-\frac{3(x-v_0t)^2}{a_1^2}\right]\times\exp\left(-\frac{3y^2}{b^2}\right)\times\exp\left(-\frac{3z^2}{c^2}\right),\ (x-v_0t)\geqslant 0 \quad (10)$$

$$q_r(x,y,z)=\frac{6\sqrt{3}(f_rQ)}{\pi\sqrt{\pi}a_2bc}\exp\left[-\frac{3(x-v_0t)^2}{a_2^2}\right]\times\exp\left(-\frac{3y^2}{b^2}\right)\times\exp\left(-\frac{3z^2}{c^2}\right),\ (x-v_0t)<0 \quad (11)$$

式中：a_1，a_2，b，c 为热源形状参数；f_f，f_r 为热流密度在熔池前后的分配系数，$f_f+f_r=2$；Q 为有效热输入；v_0 为焊接速度.

双椭球体热流模式是以体热源的形式施加到工件中的，考虑了电弧热流沿板厚方向的分布. 与面热源相比，更符合 GMAW 热过程的特点.

2.2 过热熔滴的热焓

由于射流过渡时熔滴具有较大的动量，进入熔池后一直到达熔池底部，此过程极短，假设熔滴从熔池表面运动到熔池底部时过热度不会降低，即熔滴一旦进入熔池便在特定区域内均匀分布. 文献[4]指出，熔滴对熔池的能量主要集中在焊丝正下方最大长度为 2.51 mm，最大宽度为 1.20 mm，最大深度为 0.66 mm 的区域内. 现把过热熔滴带入熔池的热量等效为该区域的均匀体热源，与双椭球的电弧热流相迭加.

熔滴热焓量 S_d 可根据焊接电流计算[4]，得

$$S_d=0.5519I+1715.1801 \quad (12)$$

焊接低碳钢时熔池的平均热焓量 S_p 为

$$S_p=1.45\sim1.61 \quad (13)$$

由此可得熔滴带入熔池的热焓量为

$$S_2=S_d-S_p \quad (14)$$

3 结果与分析

选用直径为 1.2 mm 的低碳钢焊丝，直流反接，对 6 mm 厚的低碳钢 Q195 试件进行 GMAW 焊接，采用的保护气体为 Ar 气和 2% 的 O_2 气体. 焊接电流 240 A，电弧电压 25 V，焊接速度 430 mm/min. 计算结果表明，电弧引燃后，约经过 5 s 焊接过程达到宏观准稳态.

图 1 给出了从引弧到准稳态这一过程中熔池形状的瞬时演变过程，分别从工件上表面、纵截面、横截面来表征其变化规律. 图 1a 描述了工件上表面

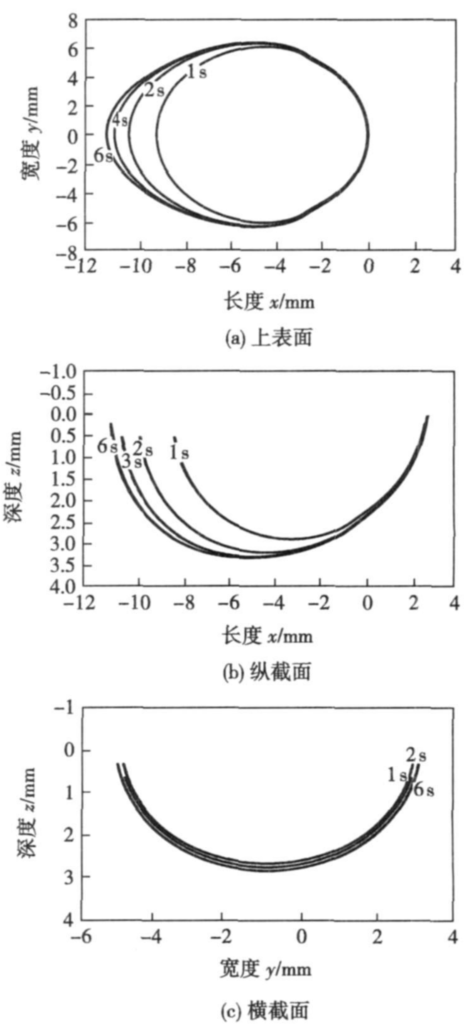

图 1 熔池形状的动态演变

Fig. 1 Transient variation of weld pool geometry

熔池形状的动态演变. 熔池刚开始形成时, 形状类似椭圆, 后拖不明显. 随着时间的延长, 熔池后方逐渐产生后拖的尾部, 而熔池的前方变化不明显. 熔池的形状沿焊接方向被拉长. 图 1b描述了工件纵截面熔池形状的动态演变. 随焊接时间的延长, 熔深和熔池长度均变大. 熔池后方的形状变化仍较前方明显, 这是由于电弧向前运动, 对其前方的工件加热时间短, 热输入少, 所以变化较大. 而电弧对其后方的工件相当于有一个预热的过程, 加热时间较长, 热输入大, 所以温度梯度会较小, 变化也较小. 图 1c描述了工件横截面熔池形状的动态演变.

图 2是熔池自由表面变形的动态演变示意图, 分别从纵截面和横截面来表征其变化规律. 图 3是熔池表面变形动态演变的三维视图, 分别给出了焊接过程中第一秒、第三秒、第五秒的熔池形状的三维视图. 由图 2和图 3可以看出, 由于熔滴冲击力和电弧压力等的作用, 电弧正下方的熔池表面下凹, 低于未熔化的工件表面. 由于这一凹陷变形以及填充金属的加入, 电弧后方的熔池表面隆起, 高于未融化的工件表面, 因此形成了凝固后的焊缝余高部分. 计算所得熔池表面的下凹变形深而宽, 最大下凹为 2.90 mm, 隆起高度为 2.18 mm.

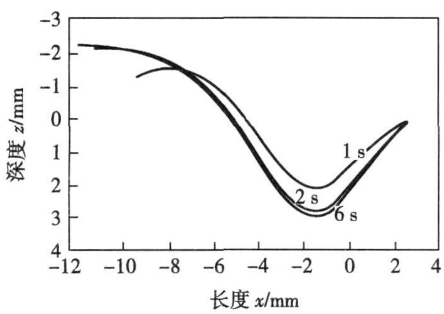

(a) 纵截面

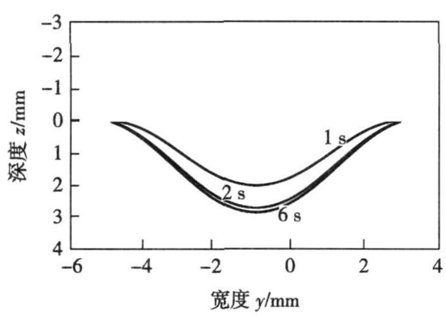

(b) 横截面

图 2 熔池自由表面变形的动态演变

Fig. 2 Dynamic development of free surfaces deformation

图 4是焊缝形状尺寸的预测结果与试验结果的比较. 图中熔深和熔宽与实际结果相差不大, 但熔合线走向仍然存在一定差异, 这是由双椭球热源模

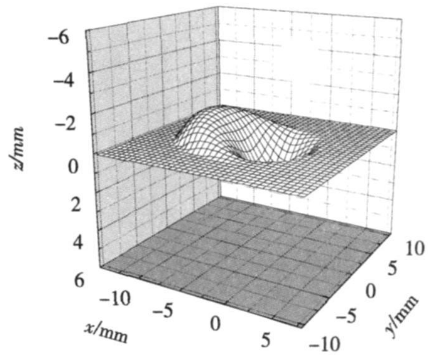

(a) t =1.0 s 熔池表面变形三维视图

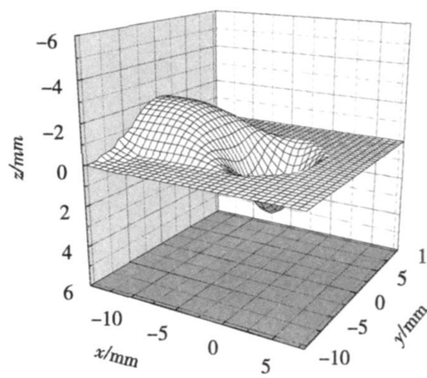

(b) t =3.0 s 熔池表面变形三维视图

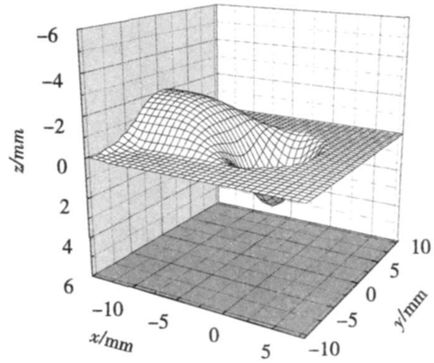

(c) t =5.0 s 熔池表面变形三维视图

图 3 熔池表面变形的三维视图

Fig. 3 Three-dimensional weld pool surfaces

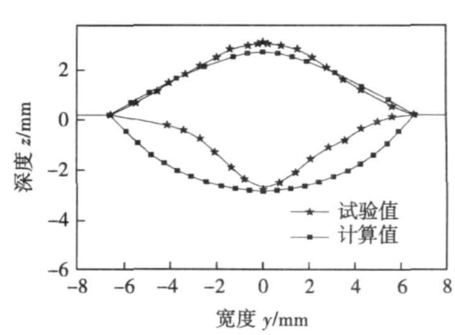

图 4 焊缝形状尺寸的预测结果与试验结果对比

Fig. 4 Comparison between calculated and experimental results

型内部热流分布所致．尚需在日后的工作中不断改进．

4 结 论

（1）采用双椭球体热源模式，把过热熔滴带入熔池的热量处理为特定区域内的均匀热源，建立了运动电弧作用下 GMAW 焊接 6 mm 低碳钢试件焊接热过程的数值模型．

（2）对 GMAW 从起焊到准稳态的焊接熔池形状和表面变形进行了预测，达到宏观准稳态时计算所得的焊缝形状尺寸与试验结果基本吻合．

参考文献：

[1] Wu C S, Dorn L. Prediction of surface depression of a tungsten inert gas weld pool in the full penetration condition[J]. Journal of Engineering Manufacture, 1995, 209(2): 221－226.

[2] Fan H G, Tsai H L, Na S J. Heat transfer and fluid flow in a partially or fully penetrated weld pool in gas tungsten arc welding[J]. International Journal of Heat and Mass Transfer, 2001, 44(2): 417－428.

[3] Choo R T C, Szekely J, Westhoff R C. Modeling of high-current arcs with emphasis on free surface phenomena in the weld pool[J]. Welding Journal, 1990, 69(9): 346s－361s.

[4] Zhao Ming, Li Ruiying. Numerical analysis of dynamic variation of weld pool geometry in fully-penetrated TIG welding[J]. China Welding, 2008, 17(2): 47－53.

作者简介：孙永兴，男，1964 年出生，硕士，教授，硕士生导师．主要研究方向为焊接设备及其自动化、焊接热过程的数值模拟．发表论文 10 余篇．

Email: taiyangyu0631@163.com

[上接第 38 页]

[4] Zhang L, Wang Z G, Shang J K. Current-induced weakening of Sn3.5Ag0.7Cu Pb-free solder joints[J]. Scripta Materialia, 2007, 56(5): 381－384.

[5] 董文兴，郝 虎，史耀武，等．稀土改性的 Sn-58Bi 低温无铅钎料[J]．电子元件与材料，2007，26(6)：21－24.
Dong Wenxing, Hao Hu, Shi Yaowu, et al. Rare earths modified Sn-58Bi low-temperature lead-free solder[J]. Electronic Components and Materials, 2007, 26(6): 21－24.

[6] Miao H W, Duh J G. Microstructure evolution in Sn-Bi and Sn-Bi-Cu solder joints under thermal aging[J]. Materials Chemistry and Physics, 2001, 71(3): 255－271.

[7] Xu G C, He H W, Guo F. Temperature-dependent phase segregation in Cu/42Sn-58Bi/Cu reaction couples under high current density[J]. Journal of Electronic Materials, 2008, 38(2): 273－283.

[8] He H W, Xu G C, Hao H, et al. Electromigration in lead-free Sn3.8Ag0.7Cu solder reaction couple[C] // 8th International Conference on Electronic Packaging Technology, Shanghai, China, 2007: 225－229.

[9] Chen C M, Huang C C. Atomic migration in eutectic SnBi solder alloys due to current stressing[J]. Journal of Materials Research, 2008, 23(4): 1051－1056.

[10] Chen C M, Chen L T, Lin Y S. Electromigration-induced Bi segregation in eutectic SnBi solder joint[J]. Journal of Electronic Materials, 2007, 36(2): 168－172.

作者简介：何洪文，男，1979 年出生，博士．研究方向为先进电子连接材料及技术．发表论文 10 余篇．

Email: hhw@emails.bjut.edu.cn

main driving force for Bi diffusion and migration.

Key words: electromigration; Bi layer; current density; Joule heating

Numerical simulation of weld pool geometry and surfaces deformation in GMAW SUN Yongxing[1], ZHAI Lei[1], ZHAO Ming[2] (1. College of Mechanical & Electronic Engineering, China University of Petroleum, Dongying 257061, China; 2. Shengli Engineering & Consulting Co., Ltd., Dongying 257026, China). p 39—42

Abstract: Numerical simulation analysis model for gas metal arc welding (GMAW) was created in the course of the welding heat based on Visual Fortran. A double ellipsoid heat source mode was adopted to depict the distribution of a moving GMAW arc. Transient variations of weld pool geometry and free surfaces deformation were predicted and verified. The results show that the calculated width and depth of molten pool are in agreement with those of the experimental results.

Key words: gas metal arc welding; free surfaces deformation; double ellipsoid heat source; numerical analysis

Microstructure and properties of WC-4Co ESD coating of cast steel roll WANG Jiansheng[1,2], MENG Huimin[2], ZHANG Ruizhu[1], YAN Dakao[1] (1. North China Institute of Water Conservancy and Hydroelectric Power, Zhengzhou 450011, China; 2. College of Materials Science and Engineering, University of Science and Technology Beijing, Beijing 100083, China). p 43—46

Abstract: WC-4Co electrode material is deposited on the surface of cast steel roll by electro-spark deposition (ESD). The microstructure and wear resistance of the coating are investigated. The results show that the coating consists of Fe_3W_3C, Co_3W_3C, Fe and SiC phases, and the coating bonded with cast steel roll substrate is well metallurgical. The phases of Fe_3W_3C and Co_3W_3C distribute dispersedly in the coating with the extra-fine structure. The average hardness of the coating is 1 617.2 HV. The resistance performance of the coating is 2.1 times higher than that of the cast steel substrate. The wear mechanism is adhesion wear, fatigue wear, oxidization wear and abrasive wear, but the main wear mechanism is fatigue wear and abrasive wear.

Key words: electro-spark deposition; WC-4Co; cast steel roll; microstructure; wear resistance

Analysis of microstructure and properties of TiC-WC reinforced Ni-based composite coating by argon arc cladding WANG Yongdong, WANG Zhenting, ZHANG Haijun, ZHU Yan (Department of Material Science and Technology, Heilongjiang Institute of Science and Technology, Harbin 150022, China). p 47—49

Abstract: Ni-based composite coating reinforced with the pre-alloyed powder of Ni60A, WC, Ti and C was prepared on the surface of Q235 steel by means of argon arc cladding technique. The microstructure was investigated by using optical microscope, scanning electron microscope and X-ray diffraction. The results show that the main phases of coating are TiC, (Ti,W)C, γ-Ni dendrite structure and $M_{23}C_6$ eutectic structure. The grain of TiC is fine, which size is about 1.5 μm, and distributes uniformly. The test results of micro-hardness and wear resistance show that the micro-hardness is improved about 4 times compared with that of the Q235 steel. The argon arc cladding composite coating has high hardness and excellent wear resistance under dry sliding wear test conditions.

Key words: argon arc cladding; composite coating; micro-hardness; wear resistance

Ultrasonic pulse tungsten inert-gas arc welding of Ti-6Al-4V alloy ZHOU Shuiliang[1], ZHAO Haitao[1], QI Bojin[2] (1. Aeronautical Key Laboratory for Aviation Joining Technology, Beijing Aeronautical Manufacturing Technology Research Institute, Beijing 100024, China; 2. School of Mechanical Engineering and Automation, Beijing University of Aeronautics & Astronautics, Beijing 100191, China). p 50—52

Abstract: Ti-6Al-4V alloy was welded by conventional tungsten inert-gas arc welding (TIG) and ultra-sonic pulse TIG welding (U-TIG), respectively. The microstructure of the joint was analyzed by means of optical microscope, scanning electron microscope and X-ray diffraction to study the relationship between the macro-properties and the microstructure of the joint. The results show that U-TIG welding can reduce pores of joint. With the increment of pulse frequency, the microstructure becomes finer and finer and is inclined to equiaxed crystal, while pulse frequency is 45 kHz, the effect of grain refinement is the best. Moreover, the properties of joint by U-TIG welding are improved compared with that of conventional TIG. The tensile fractures of the joints welded by TIG and U-TIG all present the character of quasi-cleavage crack, but the cellular dendrite depredation is not observed obviously in U-TIG joint.

Key words: ultra-sonic pulse TIG welding; conventional TIG welding; Ti-6Al-4V titanium alloy

Optimization design of twin-wire welding temperature field algorithm procedures YANG Xiuzhi[1], YU Shengfu[1], YAO Rungang[2] (1. Materials College, Huazhong University of Science and Technology, Wuhan 430070, China; 2. Materials Institute 725 of Luoyang Ship, Luoyang 471039, China). p 53—56

Abstract: The temperature field of the twin-wire submerged arc welding was analyzed by finite element software ANSYS of secondary development. The calculation and loading of heat of mobile heat source were programmed by ANSYS parametric design language. In particular, by the use of vector, the calculation and loading operation were simplified and the efficiency of simulation was improved. The experiments verify that the algorithm of heat load makes simulation time and calculation reduce, and the algorithm is feasible and efficient. This algorithm can be applied to the thermal calculation and loading of temperature field for multiple wire welding.

Key words: twin-wire submerged arc welding; mobile source; algorithm; vector

Effect of Mn content on CGHAZ microstructure and properties of large heat input welding in ship steels LUO Xiaobing[1,2], SU Hang[2], YANG Caifu[2], CHAI Feng[2], YUAN Xiaomin[1] (1. School of Materials Science and Engineering, Anhui University of Technology, Maanshan 243002, China; 2. Institu-